Scientific Research Publishing

Materials Sciences and Applications, 2023, 14, 346-361
https://www.scirp.org/journal/msa
ISSN Online: 2153-1188
ISSN Print: 2153-117X

Incorporation of Nano-Zinc Oxide in Lamellar Zirconium Phosphate: Synthesis and Characterization

Danielle Mattos Mariano, Daniela França Silva Freitas, Gerson Alberto Valencia Albitres, Luis Claudio Mendes*, Maria Ines Bruno Tavares

Instituto de Macromoléculas Professora Eloisa Mano, Centro de Tecnologia, Universidade Federal do Rio de Janeiro, Rio de Janeiro, Brazil
Email: *lcmendes@ima.ufrj.br

How to cite this paper: Mariano, D.M., Freitas, D.F.S., Albitres, G.A.V., Mendes, L.C. and Tavares, M.I.B. (2023) Incorporation of Nano-Zinc Oxide in Lamellar Zirconium Phosphate: Synthesis and Characterization. *Materials Sciences and Applications*, **14**, 346-361.
https://doi.org/10.4236/msa.2023.146022

Received: May 9, 2023
Accepted: June 23, 2023
Published: June 26, 2023

Abstract

In order to provide ultraviolet barrier, antifungal and antibacterial properties, nano-zinc oxide (ZnO) was added to lamellar zirconium phosphate (ZrP). The phosphate was synthesized via reaction of zirconium oxychloride octahydrate and phosphoric acid following its chemical modification with *Jeffamine* and nano-ZnO. Diffractometric, morphological, thermal, structural and relaxometric evaluations were conducted. Fourier transform infrared spectroscopy (FTIR) revealed increase of the area between 4000 - 3000 cm^{-1} due to the formation of ionic specie PO^{-} $^{+}NH_3$-[C-(H)(CH_3)-CH_2-O-(C-(H)(CH_3)-CH_2-O)$_8$-(CH_2-CH_2-O-CH_3)] and nano-ZnO particles. Wide-angle X-ray diffraction indicated that intercalation of *Jeffamine* was successful. Thermogravimetry confirmed that nano-ZnO particle forced the expulsion of *Jeffamine* outside ZrP galleries. Scanning electron microscopy evidenced the *Jeffamine* intercalation and sample heterogeneity. Hydrogen molecular relaxation indicated the increase of molecular rigidity owing to the formation of ionic specie and the addition of nano-ZnO particles. It was postulated that a multifunctional and miscellaneous material constituted by as prepared ZrP, some delaminated ZrP platelets and nano-ZnO particles was achieved. The material has potential for usage as filler in polymeric composites.

Keywords

Lamellar Zirconium Phosphate, *Jeffamine*, Nano-Zinc Oxide, Intercalation

1. Introduction

Nano-zinc oxide as nanoparticle possesses many attributes. Prominent physical and chemical properties make it a suitable candidate for applications in the elec-

tronic, pharmaceutical, cosmetic, personal care, civil construction and many other industries. Interest has been given to applications related to its bactericidal properties. The investigation of ZnO nanofiller as shielding against ultraviolet radiation in polymer blend of recycled poly (ethylene terephthalate)/polycarbonate (rPET/PC) was carried out by Pires and co-authors. The authors concluded that in some extent the nZnO attenuated the matrix damage being a promising ultraviolet (UV) barrier agent [1]. Synergic action of ZnO nanoparticle and gamma-radiation in recycled polycarbonate as barrier against ultraviolet radiation was studied. The authors considered that the combined action of nanofiller and irradiation as barrier to UV was satisfactory [2]. The action of ZnO nanoparticles antibacterial agent was reviewed. The mechanisms and its interaction with a diversity of microbes were approached [3]. Kavitha *et al.* published a review with detailed approach on antibacterial capacity of ZnO nanoparticles [4]. Zirconium and titanium phosphate (ZrP and TiP) are the most studied in the field of lamellar metal transition phosphates. They presented combination of tetrahedral and octahedral as lamellar structural arrangement. This permits a wide range of physical and chemical modifications [5]. Copper-containing titanium phosphate was developed by Yerga *et al.* with electrocatalytic effect towards the oxidation of glucose [6]. Searching tribological application and dispersion stability in lubricating oil, Jiang *et al.* reported the expansion of zirconium phosphate galleries with amines. The well-dispersed nanosheets decreased the coefficient of friction and pin volume loss resulting in protection of the rubbing surface [7]. Gentamicin was intercalated inside the zirconium phosphate. The filler was embedded in nanocomposites based on polymer blend of poly(ethylene oxide terephthalate)/poly(butylene terephthalate). The system was studied as functional biocomposites as drug carrier [8]. Ramos-Garcés and Colón presented an overview about of the advancements of zirconium phosphate as inorganic support for the electrocatalysis in oxygen evolution reaction [9]. Layered nanocrystalline zirconium (IV) phosphonate-phosphate was synthesized searching an ion exchange material with selectivity for terbium^{3+} [10]. Hexagonal, platelets, rods, cubes and spheres of ZrP were synthesized following their modification with Co (II) and Ni (II) cations in order to investigate their electrochemical oxygen evolution reaction behavior. Maximum ion exchange capacity varied according to ZrP morphology and kind of cation chosen [11]. Synthesis and amine intercalation of lamellar zirconium phosphate (ZrP) was experienced by Mariano *et al.* using ether-amine oligomer (EA) as intercalator agent at different EA:ZrP ratios. The material was thought for using in the controlling release of drugs [12]. Aiming application in the textile industry, Albitres *et al.* synthesized α-titanium phosphate (α-TiP). Following, they performed its intercalation with two different long chain amines with the aid of short amine. Raman spectroscopy revealed chemical modification of α-TiP [13]. To develop a nanocarrier material, Carvalho *et al.* synthesized and modified α-zirconium phosphate (α-ZrP) with zinc gluconate (ZnG) as control drug delivery. The authors stated that the strong interaction between ZrP and ZnG occurred [14]. Octadecylamine (Oct) was experienced as intercalating agent for

α-zirconium phosphate (*α*-ZrP) by ethanol/water at different amine:phosphate ratios (0.5:1, 1:1, and 2:1). The intercalation revealed the presence of free and bonded amine besides the influence on the amine melting temperature [15].

The purpose of this work led in consideration the nano-ZnO characteristics as ultraviolet barrier, antifungal and antibacterial. In this context, we synthesized ZrP following its chemical modification with *Jeffamine* and nano-ZnO. Structural, crystallographic, thermal, morphologic, and molecular mobility characteristics were assessed. A multifunctional and miscellaneous material was reached potentially applicable for polymeric composites.

2. Experimental

Materials

Phosphoric acid (H_3PO_4), zirconium (IV) oxide chloride 8-hydrate ($ZrOCl_2 \cdot 8H_2O$), *Jeffamine*® M-600 (≈600 g/mol, backbone propylene oxide:ethylene oxide, 9:1) ethyl alcohol, zinc oxide (ZnO, <100 nm) by Sigma-Aldrich Co. *Jeffamine*® was designated as ether-amine oligomer and its acronym was E-A.

Synthesis of layered zirconium phosphate

By direct precipitation, phosphoric acid solution equal 12 M was mixed in zirconium oxychloride at ratio Zr/P = 18, kept under reflux at 110˚C, under stirring, for 24 hours. After centrifugation, the solid was washed successively until attaining pH around 6 [15].

Chemical modification of layered zirconium phosphate

Chemical modification was performed in two steps. In the first step, *Jeffamine* was added in different proportions of amine:phosphate (0.5:1, 1:1, 2:1). The description of the experimental procedure was reported in elsewhere [16]. It was decided to use the material with 0.5:1 ratio which was designated as E-A/ZrP. Following, this sample was chemically modified with nano-ZnO at proportion 1:1 ratio. Nano-ZnO was dispersed in ethanol and slowly drip in E-A/ZrP ethanol dispersion, at 25˚C, under stirring, for 24 hours. Subsequently, washed with water and dried at 110˚C, until constant weight. A sketch of the experimental procedure is showed in **Figure 1**.

Wide-angle X-ray diffraction (WAXD)

Rigaku equipment, model Ultima IV was used at CuK*α* radiation with wavelength (1.5418 Å) Ni filter, 30 kV voltage and current of 15 mA, 2θ between 2˚ - 50˚ and resolution of 0.05˚. Interlayer spacing was evaluated by Bragg equation $n = 2d_{hkl}\,\text{sen}\,\theta$ (n—diffraction order, d_{hkl}—interlayer spacing, θ—diffraction angle). Debye-Scherrer equation $\tau = K * \lambda/\beta * \cos\theta$ (K = proportionality constant, 0.9; λ = mean value of the wavelength of Cu radiation in the apparatus, 1.5418 Å; β = peak width at half height (in radians); θ = half of the 2θ value from crystalline peak) was applied for determining crystal size.

Field emission scanning electron microscopy (SEM) and Energy Dispersive Spectroscopy (EDS)

SEM analysis was performed at Tescan field emission microscope, model

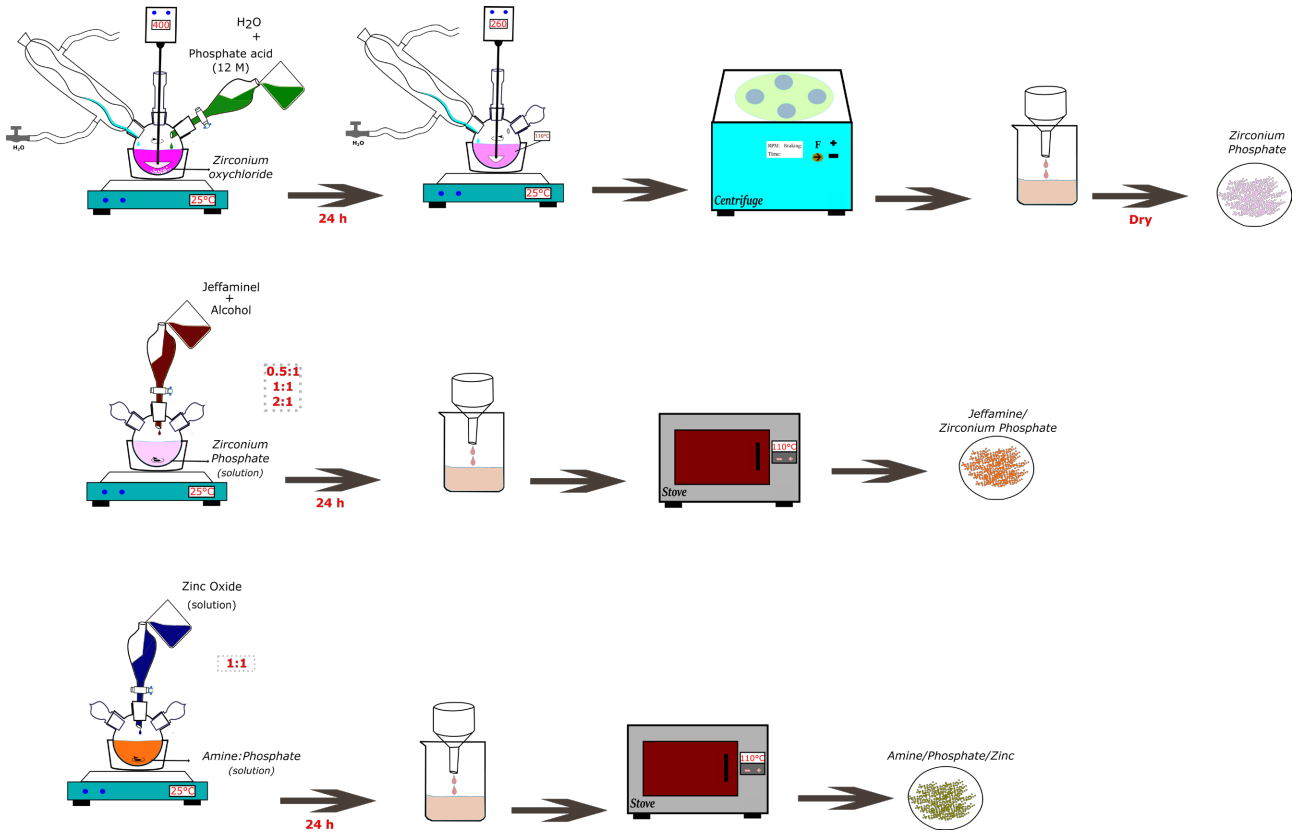

Figure 1. Sketch of the ZrP synthesis and chemical modification.

MIRA 4 LMU, cannon FEG Schottky (Field Emission Scanning Electron Microscope). The SEM has as an accessory an EDS detector with a 30 mm^2 Si_3N_4 window and a resolution lower than 129 eV for the MnKα emission line, used to mapping test.

***Thermogravimetry* (*TGA*)**

Thermogravimetry was carried out in TA instrument, model Q500. The analysis was conducted from 10˚C to 700˚C, at 10˚C/min, with nitrogen as carrying gas. Mass loss and derivative curves were assessed.

***Fourier transform infrared spectroscopy* (*FTIR*)**

In Perkin Elmer equipment, model Frontier the infrared spectroscopy was performed at range of 4000 - 400 cm^{-1} with 50 scans and 4 cm^{-1} of resolution, by using KBr disk.

***Hydrogen nuclear magnetic resonance in time domain* (*^{1}HNMRTD*)**

^{1}HNMRTD was performed in a MARAN Ultra spectrometer with an electromagnet operating at 0.54 T (Larmor frequency corresponding to 23.4 MHz for the proton), probe with an internal diameter of 18 mm, at 27˚C. The 90˚ excitation pulse was automatically calibrated to 7.5 μs. The longitudinal (T_1) relaxation time was fitted by inversion-recovery (IR). Inversion-recovery (T_1) was accomplished in the time intervals, considering forty points spaced logarithmically at a range of 0.1 to 5000 ms, with a recycle interval of 3 s and 8 accumulations [17].

3. Results and Discussion

Infrared spectroscopy (FTIR)

For better understanding, all spectra were divided at different spectral regions (Figure 2). ZrP bands at 3595, 3511 and 1617 cm^{-1} (asymmetric/symmetric bending of water in the interlayer region), 3153 cm^{-1} (stretching of the hydrogen bonding between H-O-H and P-OH group), 1250 cm^{-1} (P-O-H bending), 1112, 1074 and 1050 (PO_4 asymmetric stretching) and 980 and 968 cm^{-1} (PO_4 symmetric stretching) were registered. These attributions agreed with reported by Smith *et al.* [18]. Bands at 599 and 522 cm^{-1} were attributed to the Zr-O vibrations coinciding with published by Ran and co-authors [19]. Bands at 2972, 2931 and 2873 cm^{-1} (CH and CH_2 stretching), 1460 cm^{-1} (CH bending), 1108 and 1016 cm^{-1} (C-O-C stretching) were associated to the main absorptions of *Jeffamine* [12].

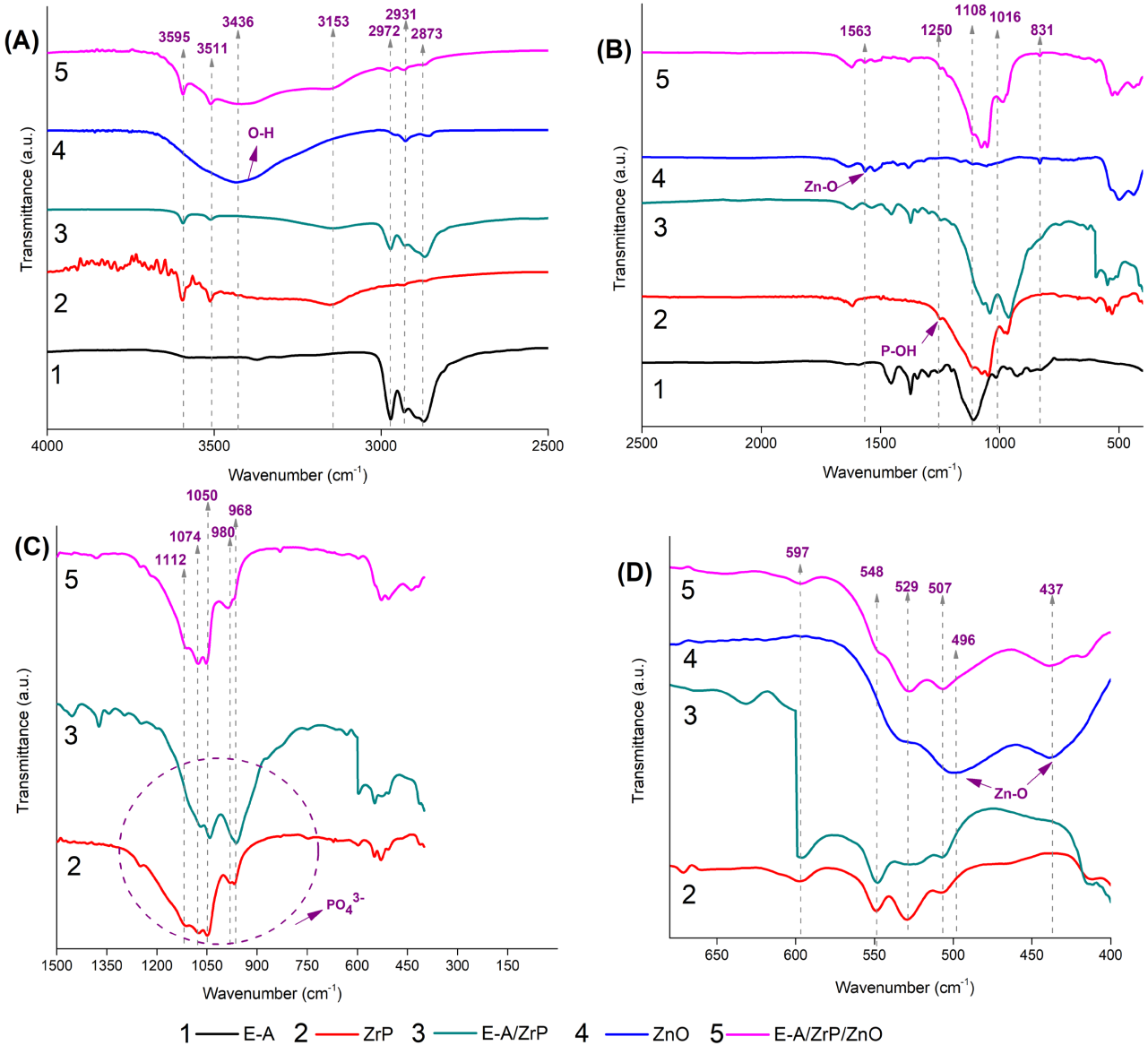

Figure 2. Infrared spectra of the *Jeffamine* and phosphates.

Jeffamine-modifying ZrP presented the ZrP characteristic bands in the 4000 - 3000 cm^{-1} spectral region. *Jeffamine* bands at 3000 - 2500 cm^{-1} and between 1500 - 1300 cm^{-1} also appeared. The ZrP band at 1250 cm^{-1} remained. At 1200 - 900 cm^{-1}, P-O (phosphate) and C-O-C (*Jeffamine*) bands overlapped but discrete shift was noticed when compared to the precursors. New band appeared at 600 - 700 cm^{-1}. Albitres *et al*. registered new bands at 1548, 1206, 1092 and 665 cm^{-1} after intercalation of *α* titanium phosphate with *Jeffamine* and ethylamine [13]. Weak vibration at 596 cm^{-1} (P-OH stretching) was reported after intercalation of layered ZrP [13] [20]. After exfoliation, sulfonic group was anchored onto ZrP. The authors registered the superposition of the S=O and P-O bands [21]. ZnO showed a broad and intense band at 3436 cm^{-1} along with a series of weak bands (1563 cm^{-1}, 1534 cm^{-1}, 2925 cm^{-1}, 2855 cm^{-1}, 1456 cm^{-1}, 1379 cm^{-1}, 1316 cm^{-1}, 1161 cm^{-1}, 1053 cm^{-1}, 831 cm^{-1}, 496 cm^{-1} and 437 cm^{-1}). The searching for works to support our results revealed that bands attribution was dependent on the starting reagent, preparation method, temperature, sample size and geometry, and mainly the lack of efficient purification of the final ZnO [22] [23] [24] [25]. The spectrum of the phosphate modified with ZnO exhibited ZrP bands at 3595; 3511; 3153; 1617 cm^{-1} already described. Bands at 1250 cm^{-1}; 1112; 1074; 1050; 980 and 968 cm^{-1} associated with P-O-H and PO_4 groups were consistent with the starting ZrP. Bands at 496 and 437 cm^{-1} related to the Zn-O stretching sharply appeared. The peak area at spectral region of 4000 - 3000 cm^{-1} (absorptions at 3595; 3511; 3153 cm^{-1} associated to the hydrogen bond of P-OH and water) and 3000 - 2500 cm^{-1} (absorptions at 2972; 2931; 2873 cm^{-1} related to the vibration of C-H and H-C-H) were measured. Table 1 depicts the calculation. Significant variations were noticed. After the addition of *Jeffamine*, the peak area at region 4000 - 3000 cm^{-1} showed a highlighted increase. We supposed that the variation is associated with the formation of ionic specie $PO^{-}{}^{+}NH_3$-[C-(H)(CH_3)-CH_2-O-(C-(H)(CH_3)-CH_2-O)$_8$-(CH_2-CH_2-O-CH_3)] by Brϕnsted acid-base reaction between P-O-H and H-N-H group. The addition of nano-ZnO generated high increment possibly due to OH groups on its surface. Respect to another spectral region, we postulated that its reduction would be due to the disruption of E-A-ZrP sites by nano-ZnO particles below 30 nm. Its action inducted the ejection *Jeffamine* free molecules and some delamination of the E-A-ZrP platelets.

Wide-angle X-ray diffraction (WAXD)

Table 1. Area of specified spectral region.

Sample	Spectral region 3595; 3511; 3153 cm^{-1} Area	Spectral region 2972; 2931; 2873 cm^{-1} Area
ZrP	43.31	---
E-A/ZrP	56.06	12.86
E-A/ZrP/ZnO	61.87	9.53

Figure 3 illustrates the WAXD diffraction patterns of the samples and a sketch of the assumed changes after each chemical modification. Table 2 summarizes the diffraction angle, $d_{spacing}$ and crystal size of the samples. *Jeffamine*^{TM} diffractogram (black curve) indicated an amorphous matter. ZrP (red curve) showed diffraction angles around $2\theta = 11.75$ ($d_{spacing} = 7.52$ Å), 19.89˚ and 25.04˚

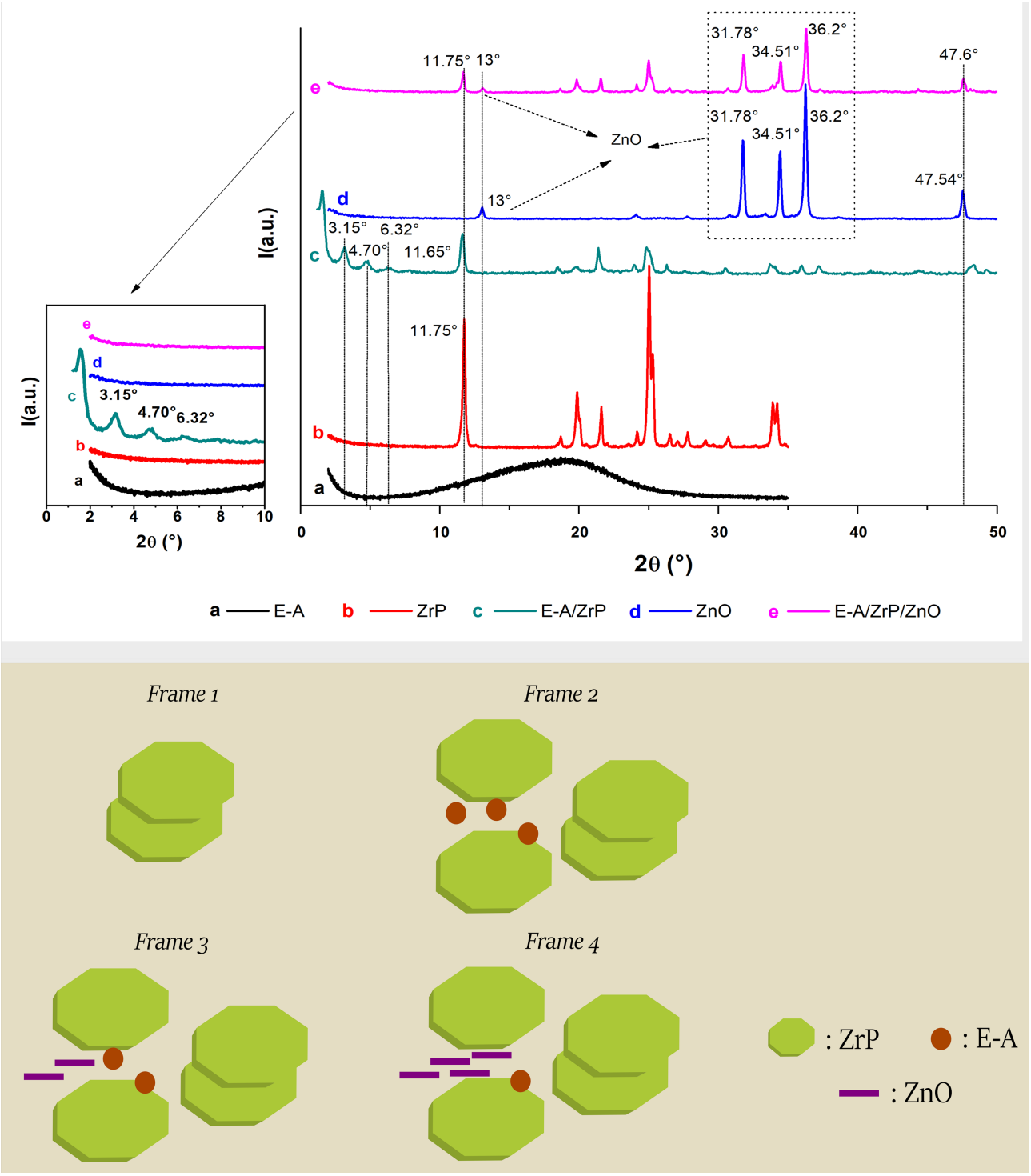

Figure 3. Diffraction pattern of the samples and a sketch of the assumed changes after ZrP chemical modifications.

Table 2. Diffraction angle, $d_{spacing}$ and crystal size of as prepared and modified ZrP.

Sample	ZrP 2θ (˚)	New ZrP 2θ (˚)	$d_{spacing}$ (Å)	τ (nm)
ZrP	11.75	---	7.53	302
E-A/ZrP	11.62	6.32; 4.70; 3.15	7.53; 13.97; 18.79; 28.02*	237
E-A/ZrP/ZnO	11.68	---	7.53	270

*Sequentially, ZrP and *Jeffamine*-modifying ZrP $d_{spacing}$ values.

corresponding to crystalline plane (002), (110) and (112) [Garcia *et al.* and Han *et al.*] [26] [27]. At E-A/ZrP diffraction pattern (light blue curve), *hkl* plane of ZrP remained but new diffraction angles appeared at 6.32˚, 4.70˚ and 3.15˚ (magnified laterally). These mixing of intercalated phases mean that more probably in each one there is variation in *Jeffamine* alignment. Similar result was published by Kale *et al.* using ethylenediamine as intercalator [28]. ZnO diffraction pattern (dark blue curve) presented 2θ around 31.78˚, 34.5˚, 36.2˚ and 47.6˚ corresponding crystallographic plane (100), (002), (101) e (102), respectively, as published by Mallakpour and Javadpour [29]. In the E-A/ZrP/ZnO diffraction pattern (pink curve), the absence of the diffraction angles below 10˚, the diffraction angles of ZrP and zinc oxide were depicted. The presence *Jeffamine* increased the ZrP $d_{spacing}$ up to fourfold. Crystal size of ZrP decreased dimension by consecutive addition of *Jeffamine* and nano-ZnO. With respect to the ZnO, the supplier stated that ZnO particle size is below to 100 nm but the experimental technique for its determination and range of size were not released. The addition of induced the disappearance of diffraction angles below 10˚. A reasonable explanation would be that the E-A-ZrP intercalated sites were undone by nano-ZnO particles below 30 nm ejecting *Jeffamine* molecules outside. The fragmentation of E-A-ZrP structure was evidenced by the reduction of crystal size. At frame 1, the arrangement of as prepared zirconium phosphate can be seen. Frame 2 represents the entrance of the *Jeffamine* molecules into ZrP galleries. The lamellar spacing was increased by formation of the ionic specie $PO^{-}\ ^{+}N_3H$-[C-(H)(CH_3)-CH_2-O-(C-(H)(CH_3)-CH_2-O)$_8$-(CH_2-CH_2-O-CH_3)]. Frame 3 depicts the action of nano-ZnO particle below 30 nm provoking the expulsion of E-A molecules outside and the delamination of E-A-ZrP sites. Then, we assumed that the final product (frame 4) is a miscellaneous material constituted by as prepared ZrP, some delaminated ZrP platelets and ZnO particles. The result is in accordance with the FTIR analysis.

Thermogravimetry (TGA)

Figure 4 shows the mass loss and derivative curves of samples. Table 3 discloses the degradation temperature and the amount of mass loss for each step. *Jeffamine* displayed one step of mass loss with maximum around 299˚C. Three thermal degradation decays were revealed by α-ZrP. The first one was located between 100˚C - 200˚C (T_{max} = 135˚C) attributed to the release of adsorbed water. The two others corresponded to the dehydroxylation reaction (T_{max} = 466˚C) of the hydroxyl groups attached to the phosphorus atoms and the chemical

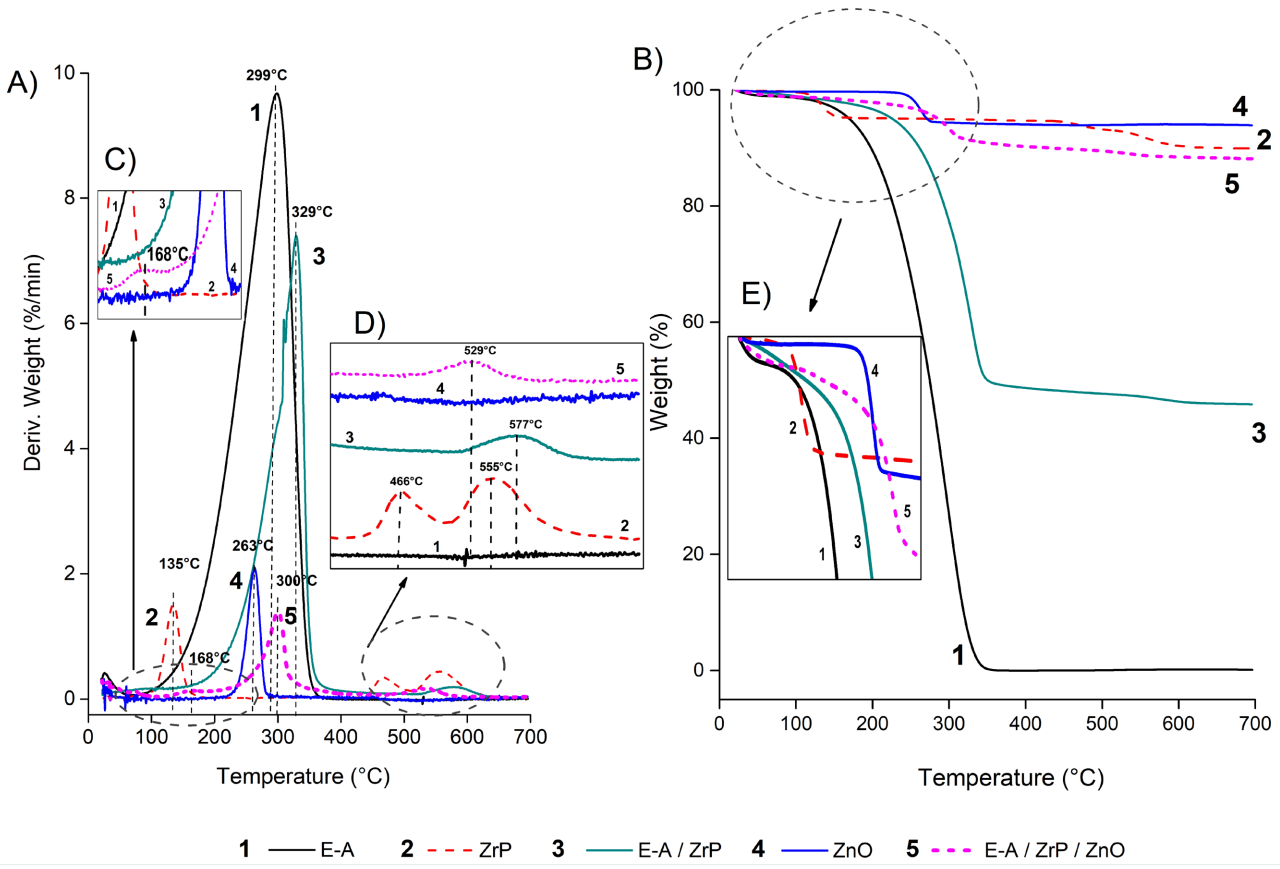

Figure 4. TGA mass loss and derivative curves of precursors and modified phosphates: (A) mass loss; (B) derivative; (C) amplified derivative (100˚C - 300˚C); (D) amplified derivative (400˚C - 700˚C) and (E) amplified mass loss (0˚C - 350˚C)

Table 3. TGA data of the precursor and modified phosphates.

Sample	T_{max1}/˚C	T_{max2}/˚C	T_{max3}/˚C	Residue/%
E-A	299 (99)	---	---	0.1
ZrP	135 (5)	466 (2)	555 (3)	90
E-A/ZrP	329 (52)	577 (2)	---	46
ZnO	263 (6)	---	---	94
E-A/ZrP/ZnO	168 (1)	300 (8)	529 (2)	89

(in parentheses, the mass loss percentage).

transformation of phosphate to pyrophosphate (T_{max} = 555˚C), respectively. Similar result was reported by Mariano and co-authors [12]. *Jeffamine*-modifying ZrP presented a decay around 300˚C (T_{max} = 329˚C) ascribed to the thermal degradation amine molecules (free and bonded). We understood that the absence of dehydroxylation step showed the effectiveness of amine intercalation as pointed out elsewhere [12]. The result is agreement with Kale *et al.* reporting intercalation of ZrP with ethylenediamine [28]. The second thermal degradation decay was related to the conversion of phosphate to pyrophosphate shifted to higher temperature (T_{max} = 577˚C). ZnO presented a unique decay (T_{max} = 268˚C) being

imputed to the release of water from crystalline lattice. As seen in infrared evaluation, herein the ZnO degradation steps revealed disagreement. Routes of synthesis, precursors and purification could be the reasons for this inconsistency [23] [30] [31] [32]. E-A/ZrP/ZnO showed 3 steps of degradation. The first one around 170˚C was attributed to ZrP water releasing. Around 300˚C, we supposed that the 8% of mass loss jointly represented the water from ZnO crystalline lattice (6%) plus the amine portion of ionic specie PO^{-} $^{+}NH_3$-[C-(H)(CH_3)-CH_2-O-(C-(H)(CH_3)-CH_2-O)$_8$-(CH_2-CH_2-O-CH_3)] (2%). The third step was related to the conversion of phosphate to pyrophosphate. The result agrees with the postulated at FTIR and WAXD evaluations. The final product is a multifunctional material encompassing as prepared ZrP, some delaminated ZrP platelets and ZnO particles.

Field emission scanning electron microscopy (SEM) and Energy Dispersive Spectroscopy (EDS)

Figure 5(A), **Figure 5(E)** depict the SEM images of ZrP and EDS evaluation. As prepared ZrP (**Figure 5(A)**) presents as a series of hexagonal structures with some agglomeration and then without homogeneity in diameter and thickness. Similarly, Ramos-Garcés *et al.* synthesized and modified ZrP with metal attained agglomerated ZrP with varied morphology—hexagonal, rod-like, cube-like, and spherical [11]. EDS evaluation (**Figure 5(E)**) revealed its elemental composition. The percentage of zirconium, oxygen and phosphorus are in good agreement with the chemical formula [$Zr(HPO_4)_2{\cdot}2H_2O$] representing the phosphate structure reported by Silva *et al.* in the work related to zirconium phosphate organically intercalated/exfoliated with octadecylamine [15]. **Figure 5(B)**, **Figure 5(F)** show the SEM images and EDS of E-A/ZrP. The image clearly confirms the hexagonal structure of ZrP with variation in diameter and thickness. Higher magnified image confirmed that *Jeffamine* was partially intercalated into ZrP galleries. The highlighted region shows the separation of the lamellae caused by the intercalator. This in good agreement with WAXD analysis in which partial interposition of *Jeffamine* along ZrP lamellae revealing new diffraction angles lesser than 10˚. The content of nitrogen was approximately to one detected in TGA analysis. SEM images and EDS of ZnO were depicted in **Figure 5(C)**, **Figure 5(G)**. Its morphology seems to be like agglomeration of fragmented rounded rod shape particles. Tymoszuk and Wojnarowicz reported heterogeneous shapes (rods, bodies with hexagonal base and irregular bodies) of ZnO submicron particles [33]. EDS evaluation of ZnO revealed its atomic composition. E-A/ZrP/ZnO images and EDS are shown **Figure 5(D)**, **Figure 5(H)**. Heterogeneity is sharply revealed. As prepared layered ZrP appeared as aggregate of hexagonal structures without homogeneity in diameter and thickness. Also, isolated platelets with lower thickness can be seen and could be associated with delaminated lamella from the action of ZnO. Small particle of ZnO was easily identified. These evidences corroborate the supposition in which a mixing of as prepared ZrP, some delaminated ZrP platelets and ZnO particles was attained.

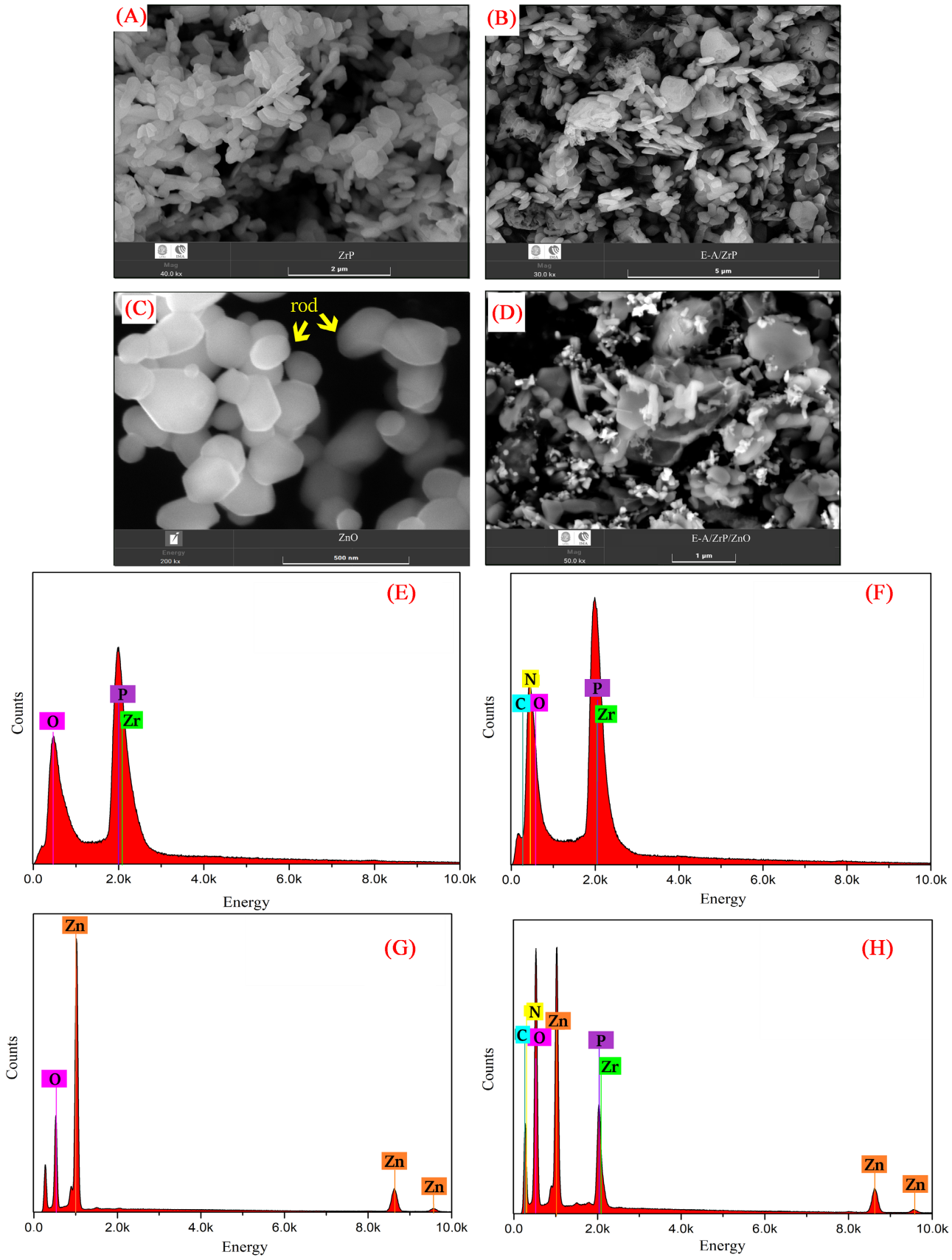

Figure 5. SEM images of the samples (A)-(D); EDS of the samples: ZrP (E), EA-ZrP (F), Zn (G), EA-ZrP-ZnO (H).

Hydrogen nuclear magnetic resonance in time domain (^{1}HNMRTD)

Figure 6 and Table 4 show the domain distribution curves and relaxation times of the samples. Domain distribution curve of *Jeffamine* showed one domain between 10^5 - 10^6 ms. ZrP presented two domains—flexible (lowest relaxation time) and rigid (highest relaxation time). The first one was related to the hydrogen relaxation of adsorbed water and free P-OH. The second one was associated to the hydrogen motion due to hydrogen bond between P-OH and water inside of its crystalline lattice. Bakhmutov and Clearfield studied the relaxation and molecular mobility of layered *α*-zirconium phosphate, at variable experiments. They reported two types of motions meaning low-frequency proton transfer and high-frequency rotation in P-OH groups [34]. The domain distribution curve of E-A/ZrP showed enlargement indicating heterogeneity as reported by Ribeiro *et al.* in article on molecular dynamics of poly (hydroxybutyrate) filled with microcrystalline cellulose [35]. The T_1H of the lowest domain decreased drastically. The entrance of *Jeffamine* inside the ZrP galleries increases the lamellar spacing favoring the hydrogen molecular mobility. The highest

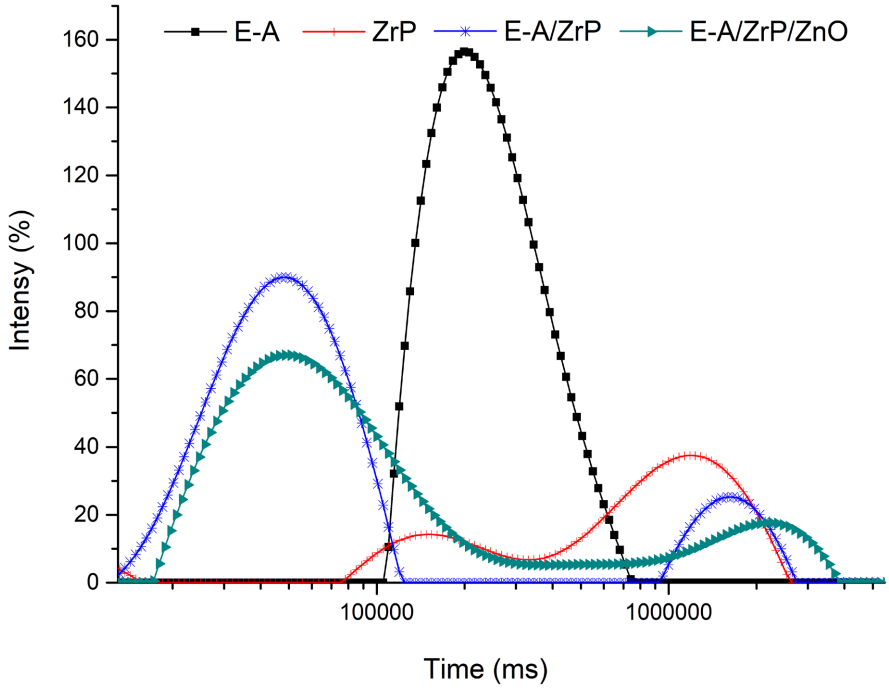

Figure 6. Domain distribution curves of the *Jeffamine*, ZrP and modified phosphates.

Table 4. T_1H of the *Jeffamine*, ZrP and modified phosphates.

Samples	T_1H (ms)	T_1H (ms)
E-A	238	---
ZrP	133	816
E-A/ZrP	48	943
E-A/ZrP/ZnO	51	1035

domain presented T_1H slightly higher. The formation of the ionic specie PO^- $^+NH_3$-[C-(H)(CH_3)-CH_2-O-(C-(H)(CH_3)-CH_2-O)$_8$-(CH_2-CH_2-O-CH_3)] hampered the hydrogen mobility in the rigid domains. The domain distribution curve of E-A/ZrP/ZnO also enlarged indicating heterogeneity. The higher T_1H value was associated to the ZnO particle which restrained the hydrogen mobility. Molecular relaxation endorsed the evidences showed in FTIR, WAXD, TGA and SEM evaluations.

4. Conclusion

This work proposed to synthesize a new filler through the combination of the inorganic and organic matters to improve ZrP properties by addition of nano-ZnO. ZrP was synthesized and chemically modified with *Jeffamine* and nano-ZnO. FTIR indicated the Brϕnsted acid-base reaction between P-O-H and H-N-H groups inducing the formation of ionic specie PO^- $^+NH_3$-[C-(H)(CH_3)-CH_2-O-(C-(H)(CH_3)-CH_2-O)$_8$-(CH_2-CH_2-O-CH_3)]. WAXD evidenced the amine intercalation and its breakdown by action of nano-ZnO which was endorsed by TGA analysis. SEM described the intercalation and the collapse of the *Jeffamine*-modifying ZrP. ZrP molecular relaxation was altered by the presence of *Jeffamine* and nano-ZnO. Multifuncional and heterogeneous material was reached.

Aknowledgements

The authors thank Fundação de Amparo à Pesquisa do Estado do Rio de Janeiro (FAPERJ), Conselho Nacional de Desenvolvimento Científico e Tecnológico (CNPq), Coordenação de Aperfeiçoamento de Pessoal de Nível Superior (CAPES) and the Universidade Federal do Rio de Janeiro staff for supporting this research.

Author's Contribution

D. M. Mariano—Conceptualization, Writing; D. F. S. Freitas—Visualization; G. A. V. Albitres—Visualization; L. C. Mendes—Conceptualization, Resources, Supervision, Writing; M. I. B. Tavares—Resources.

Conflicts of Interest

The authors declare no conflicts of interest regarding the publication of this paper.

References

[1] Pires, H.M., Mendes, L.C., Cestari, S.P., Cucinelli Neto, R.P., Rodrigues, D.C. and Mattos, G.C. (2016) nZnO as Barrier to Ultraviolet Radiation on rPET/PC Nanocomposites. *Journal of Nanoscience and Nanotechnology*, **16**, 9987-9996. https://doi.org/10.1166/jnn.2016.12080

[2] Carvalho, A.L.F., Mendes, L.C., Cestari, S.P. and Souza, M.C.L. (2017) Nanocomposites of Recycled Polycarbonate/Nano-Zinc Oxide (rPC/nZnO): Effect of Nanofiller

and Gamma-Radiation on the Properties and as Barrier against Ultraviolet Light. *Journal of Nanoscience and Nanotechnology*, **17**, 270-277. https://doi.org/10.1166/jnn.2017.12642

[3] Siddiqi, K.S., Rahman, A., Tajuddin, and Husen, A. (2018) Properties of Zinc Oxide Nanoparticles and Their Activity against Microbes. *Nanoscale Research Letters*, **13**, Article No. 141. https://doi.org/10.1186/s11671-018-2532-3

[4] Kavitha, A., Doss, A., Pole, R.P.P., Rani, T.P.K.P., Prasad, R. and Satheesh, S. (2023) A Mini Review on Plant-Mediated Zinc Oxide Nanoparticles and Their Antibacterial Potency. *Biocatalysis and Agricultural Biotechnology*, **48**, Article ID: 102654. https://doi.org/10.1016/j.bcab.2023.102654

[5] Garcia, E., Albitres, G., Freitas, D., Mariano, D. and Mendes, L. (2022) Zinc and Silver Salts-Containing Lamellar Titanium Phosphate: A Multifunctional Filler. *Materials Sciences and Applications*, **13**, 366-388. https://doi.org/10.4236/msa.2022.136021

[6] Martín-Yerga, D., Carrasco-Rodríguez, J., Fierro, J.L.G., Alonso, F.J.G. and Costa-García, A. (2017) Copper-Modified Titanium Phosphate Nanoparticles as Electrocatalyst for Glucose Detection. *Electrochimica Acta*, **229**, 102-111. https://doi.org/10.1016/j.electacta.2017.01.143

[7] Jiang, F., Sun, H., Chen, L., Lei, F. and Sun, D. (2020) Dispersion-Tribological Property Relationship in Mineral Oils Containing 2D Layered α-Zirconium Phosphate Nanoplatelets. *Friction*, **8**, 695-707. https://doi.org/10.1007/s40544-019-0294-2

[8] Bastianini, M., Scatto, M., Sisani, M., Scopece, P., Patelli, A. and Petracci, A. (2018) Innovative Composites Based on Organic Modified Zirconium Phosphate and PEOT/PBT Copolymer. *Journal of Composites Science*, **2**, Article No. 31. https://doi.org/10.3390/jcs2020031

[9] Ramos-Garcés, M.V. and Colón, J.L. (2020) Preparation of Zirconium Phosphate Nanomaterials and Their Applications as Inorganic Supports for the Oxygen Evolution Reaction. *Nanomaterials*, **10**, Article No. 822. https://doi.org/10.3390/nano10050822

[10] Terban, M.W., Shi, C., Silbernagel, R., Clearfield, A. and Billinge, S.J.L. (2017) Local Environment of Terbium(III) Ions in Layered Nanocrystalline Zirconium(IV) Phosphonate-Phosphate Ion Exchange Materials. *Inorganic Chemistry*, **56**, 8837-8846. https://doi.org/10.1021/acs.inorgchem.7b00666

[11] Ramos-Garcés, M.V., Sanchez, J., Luz-Rivera, K.L., Toro-Pedrosa, D.E.D., Jaramillo, T.F. and Colón, J.L. (2020) Morphology Control of Metal-Modified Zirconium Phosphate Support Structures for the Oxygen Evolution Reaction. *Dalton Transactions*, **49**, 3892-3900. https://doi.org/10.1039/C9DT04135D

[12] Mariano, D.M., Freitas, D.F.S., Mendes, L.C., Carvalho, A.L.F. and Ramos, F. (2019) Investigation on Structural, Morphological and Relaxometric Properties of Lamellar ZrP Modified with Long Chain Amine. *Materials Research*, **22**, 1-8. https://doi.org/10.1590/1980-5373-mr-2018-0493

[13] Albitres, G.A.V., Cestari, S.P., Freitas, D.F.S., Rodrigues, D.C., Mendes, L.C. and Neumann, R. (2020) Intercalation of α-Titanium Phosphate with Long-Chain Amine Aided by Short-Chain Amine. *Applied Nanoscience*, **10**, 907-916. https://doi.org/10.1007/s13204-019-01176-1

[14] Carvalho, A.L.F., Freitas, D.F.S., Mariano, D.M., Mattos, G.C. and Mendes, L.C. (2018) The Influence of Zinc Gluconate as an Intercalating Agent on the Structural, Thermal, Morphologic, and Molecular Mobility of Lamellar Nanofiller. *Colloid and*

Polymer Science, **296**, 1079-1086. https://doi.org/10.1007/s00396-018-4319-6

[15] Mendes, L.C., Silva, D.F., Araujo, L.J.F. and Lino, A.S. (2014) Zirconium Phosphate Organically Intercalated/Exfoliated with Long Chain Amine. *Journal of Thermal Analysis and Calorimetry*, **118**, 1461-1469. https://doi.org/10.1007/s10973-014-4056-0

[16] Mariano, D.M., Freitas, D.F.S. and Mendes, L.C. (2018) Nanocomposite of Polypropylene/Octadecylamine Lamellar-Zirconium Phosphate: Influence of Nanofiller and Screw Speed. *Journal of Composite Materials*, **52**, 701-711. https://doi.org/10.1177/0021998317713832

[17] Rodrigues, E.J.R., Cavalcante, M.P. and Tavares, M.I.B. (2016) Time Domain NMR Evaluation of Poly(vinyl alcohol) Xerogels. *Polímeros*, **26**, 221-227. https://doi.org/10.1590/0104-1428.2093

[18] Smith, A., Wan, C., Figiel, Ł., Farris, S. and McNally, T. (2020) Freestanding α-Zirconium Phosphate Based Nacre-Like Composite Films Cast from Water. *Composites Science and Technology*, **200**, Article ID: 108443. https://doi.org/10.1016/j.compscitech.2020.108443

[19] Ran, J., Xie, H., Lai, X., Li, H. and Zeng, X. (2018) Significant Improvement of Tribological Performances of Polyamide 46/Polyphenylene Oxide Alloy by Functionalized Zirconium Phosphate. *Tribology International*, **128**, 204-213. https://doi.org/10.1016/j.triboint.2018.07.019

[20] Quinelato, R.R.R., Albitres, G.A.V., Mariano, D.M., Freitas, D.F.S., Mendes, L.C., Rodrigues, D.C. and Ferreira Filho, M. (2020) Influence of Polycaprolactone and Titanium Phosphate in the Composites Based upon Recycled Polypropylene. *Journal of Thermoplastic Composite Materials*, **36**, 1264-1284. https://doi.org/10.1177/0892705720963159

[21] Mu, W., Du, S., Yu, Q., Li, X., Wei, H., Yang, Y. and Peng, S. (2019) Highly Efficient Removal of Radioactive ^{90}Sr Based on Sulfonic Acid Functionalized α-Zirconium Phosphate Nanosheets. *Chemical Engineering Journal*, **361**, 538-546. https://doi.org/10.1016/j.cej.2018.12.110

[22] Zargar, R.A., Arora, M., Alshahrani, T. and Shkir, M. (2021) Screen Printed Novel ZnO/MWCNTs Nanocomposite Thick Films. *Ceramics International*, **47**, 6084-6093. https://doi.org/10.1016/j.ceramint.2020.10.185

[23] Mallakpour, S., Abdolmaleki, A. and Moosavi, S.E. (2018) Production and Characterization of Novel Nanocomposites Based on Poly(amide-imide) Containing N-Trimellitylimido-l-alanine diacid and 4,4'-Diaminodiphenylmethan Segments Reinforced with Grafted Nano-ZnO by Citric Acid as A Biological Ligand. *Polymer Composites*, **39**, 2394-2402. https://doi.org/10.1002/pc.24221

[24] Manojkumar, U., Kaliannan, D., Srinivasan, V., Balasubramanian, B., Kamyab, H., Zainab Mussa, H., Palaniyappan, J., Mesbah, M., Chelliapan, S. and Palaninaicker, S. (2023) Green Synthesis of Nano Zinc Oxide Nanoparticles Using *Brassica oleracea var. botrytis* Leaf Extract: Photocatalytic, Antimicrobial, and Larvicidal Activity. *Chemosphere*, **323**, Article ID: 138263. https://doi.org/10.1016/j.chemosphere.2023.138263

[25] Abdelghany, T.M., Al-Rajhi, A.M.H., Yahya, R., Bakri, M.M., Al Abboud, M.A., Yahya, R., Qanash, H., Bazaid, A.S. and Salem, S.S. (2023) Phytofabrication of Zinc Oxide Nanoparticles with Advanced Characterization and Its Antioxidant, Anticancer, and Antimicrobial Activity against Pathogenic Microorganisms. *Biomass Conversion and Biorefinery*, **13**, 417-430. https://doi.org/10.1007/s13399-022-03412-1

[26] Garcia, E.E., Freitas, D.F.S., Cestari, S.P., Coval, D.R., Mendes, L.C. and Albitres, G.A.V. (2020) Zirconium Phosphate Changing Hygroscopicity of Polyamide-6 in Nanocomposites PA-6/ZrP. *Journal of Thermal Analysis and Calorimetry*, **139**, 293-303. https://doi.org/10.1007/s10973-019-08396-1

[27] Han, L., Chen, Q., Chen, H., Yu, S., Xiao, L. and Ye, Z. (2018) Synthesis and Performance of Functionalized α-Zirconium Phosphate Modified with Octadecyl Isocyanate. *Journal of Nanomaterials*, **2018**, Article ID: 5873871. https://doi.org/10.1155/2018/5873871

[28] Kale, M.B., Divakaran, N., Mubarak, S., Dhamodharan, D., Senthil, T. and Wu, L. (2019) Waterborne Polyurethane Nanocomposite Reinforced with Amine Intercalated α-Zirconium Phosphate—Study of Thermal and Mechanical Properties. *Polymer*, **186**, Article ID: 122008. https://doi.org/10.1016/j.polymer.2019.122008

[29] Mallakpour, S. and Javadpour, M. (2018) Comprehensive Study on Reinforcement of Poly(vinyl chloride) Nanocomposite Films with ZnO Nanoparticles Modified by Citric Acid and Vitamin C. *International Journal of Polymer Analysis and Characterization*, **23**, 415-429. https://doi.org/10.1080/1023666X.2018.1468175

[30] Kermani, M., Mostafapour, A., Sabouri, Z., Gheibihayat, S.M. and Darroudi, M. (2023) The Photocatalytic, Cytotoxicity, and Antibacterial Properties of Zinc Oxide Nanoparticles Synthesized Using *Trigonella foenum-graecum* L Extract. *Environmental Science and Pollution Research*, **30**, 19313-19325. https://doi.org/10.1007/s11356-022-23518-3

[31] Khan, M.Z., Taghavian, H., Fijalkowski, M., Militky, J., Tomkova, B., Venkataraman, M. and Adach, K. (2023) Effect of Microwave Power on Bactericidal and UV Protection Properties of the ZnO Nanorods Grown Cotton Fabrics. *Colloids and Surfaces A*: *Physicochemical and Engineering Aspects*, **664**, Article ID: 131135. https://doi.org/10.1016/j.colsurfa.2023.131135

[32] Arya, P.R., Abishad, P., Unni, V., Ram, P.V., Pollumahanti, N., Yasur, J., *et al.* (2023) Facile Synthesis of Silver-Zinc Oxide Nanocomposites Using *Curcuma longa* Extract and Its *in Vitro* Antimicrobial Efficacy against Multi-Drug Resistant Pathogens of Public Health Importance. *Inorganic Chemistry Communications*, **148**, Article ID: 110356. https://doi.org/10.1016/j.inoche.2022.110356

[33] Tymoszuk, A. and Wojnarowicz, J. (2020) Zinc Oxide and Zinc Oxide Nanoparticles Impact on *in Vitro* Germination and Seedling Growth in *Allium cepa* L. *Materials*, **13**, Article No. 2784. https://doi.org/10.3390/ma13122784

[34] Bakhmutov, V.I. and Clearfield, A. (2017) 31P, 1H NMR Relaxation and Molecular Mobility in Layered α Zirconium Phosphate: Variable-Temperature NMR Experiments. *The Journal of Physical Chemistry C*, **121**, 550-555. https://doi.org/10.1021/acs.jpcc.6b11247

[35] Ribeiro, F.A.S.V., Cavalcante, M.P., Tavares, M.I.B. and Aragão, A.R. (2021) Effect of Modified Microcrystalline Cellulose on Poly(3-hydroxybutyrate) Molecular Dynamics by Proton Relaxometry. *Polymers and Polymer Composites*, **29**, 553-560. https://doi.org/10.1177/0967391120926078